INSTITUT DE FRANCE
Académie des sciences

Comptes Rendus
Mécanique

Muhammad Masaud Hajjaj and Jianwei Tu

Wave attenuation study on a wide-band seismic metasurface using capped pillars

Volume 350 (2022), p. 237-254

Published online: 16 June 2022

https://doi.org/10.5802/crmeca.99

This article is licensed under the
Creative Commons Attribution 4.0 International License.
http://creativecommons.org/licenses/by/4.0/

Les Comptes Rendus. Mécanique *sont membres du Centre Mersenne pour l'édition scientifique ouverte*
www.centre-mersenne.org
e-ISSN : 1873-7234

Comptes Rendus
Mécanique
2022, 350, p. 237-254
https://doi.org/10.5802/crmeca.99

Synthesis / *Synthèse*

Wave attenuation study on a wide-band seismic metasurface using capped pillars

Muhammad Masaud Hajjaj *, [a] **and Jianwei Tu** [a]

[a] Hubei Key Laboratory of Roadway Bridge and Structure Engineering, Wuhan University of Technology, Wuhan 430070, China

E-mails: hajjaj@whut.edu.cn (M. M. Hajjaj), tujianwei@whut.edu.cn (J. Tu)

Abstract. We present the results of a numerical study on a seismic metasurface that achieves wide bandgap for low frequencies and with relatively smaller resonators. The metasurface consists of periodic concrete pillars with rigid caps supported on rubber between the caps and pillars and placed above ground. The study shows that such a metasurface creates a barrier against elastic waves having frequencies in the seismic frequency range. The results are further validated by a frequency-domain and time-transient study. The proposed metasurface configuration is simple and can be realized with readily available materials.

Keywords. Seismic metamaterial, Seismic metasurface, Local resonance, Wave propagation, Bandgaps, Capped pillars.

Manuscript received 22nd March 2021, revised 20th June 2021 and 28th October 2021, accepted 28th October 2021.

1. Introduction

Metamaterials emerged as the composite periodic medium exhibiting unusual electromagnetic properties [1], about a couple of decades ago. Ever since they have given rise to a plethora of different *meta-* concepts such as meta-materials, meta-structure [2], meta-mirror [3, 4], meta-lens [5, 6], meta-surface [7, 8], meta-wedge [9], meta-barrier [10, 11], meta-damper [12], meta-foundation [13], meta-lattice [14], etc. Based on this evolutionary path, they can be defined as artificial materials which have been structurally engineered in such a way that their geometric and topological properties overtake their chemical and atomic properties for dictating their behaviour when interacting with various physical phenomena. The phenomena for which they have been most widely studied are the wave phenomena, be it electromagnetic [1, 15], acoustic [16], elastic [17], and seismic waves [18–22] or water waves [23]. However, the scope of metamaterials has been expanded to other phenomena as well, such as heat [24]. In short, the concept has a huge potential for innovative solutions for engineering and technological problems. One such problem which has always needed new and cutting-edge solutions is the protection of

* Corresponding author.

man-made structures and infrastructure from seismic vibrations which result from seismic waves and vibrations caused by earthquakes, explosions, volcanic eruptions, heavy vehicle movements, etc. Hence, it has, in recent years, caught the attention of the seismic engineering community as well.

Seismic metamaterials, currently, are a hot research area and the researchers have produced many novel metamaterial concepts [25–44] that can provide passive protection of civil engineering structures against seismic waves. Seismic metamaterials can be a type of elastic and/or mechanical metamaterials which interact with seismic waves by the means of Bragg scattering due to their periodic structure [45] and/or local resonance [46] phenomena. For seismic and other mechanical waves, such materials can stop certain frequency ranges from propagating and create what is known as bandgaps, analogous to the energy gaps of electrons in atoms [47]. Seismic waves, due to earthquakes, travel at very low frequencies (in the range of 1–20 Hz) which gives rise to its own set of design contradictions when designing a seismic metamaterial. Metamaterials, which are desired to interact with seismic waves, might have to be of unfeasible sizes if relying solely on Bragg scattering. It has been shown that this issue can be tackled by incorporating local resonance in the material [48]. However, even with the incorporation of the local resonance in the metamaterial system, the required size of resonators may still be considerably large, resulting in larger volumes and sizes if traditional building materials i.e., concrete, steel, etc. are used. Moreover, the effectiveness of most such systems is limited to very narrow frequency bands. Overall, the major design contradictions (using the TRIZ [49] terminology) involved in the seismic metamaterial design are (i) smaller resonator or unit cell size to be more practical and feasible (ii) wide frequency bandgaps (iii) effectiveness for low-frequency ranges of seismic waves (iii) effectiveness for higher shear wave velocities and in turn Rayleigh wave velocities i.e., longer wavelengths. Therefore, presently, efforts are being made to find solutions that can resolve all of those contradictions simultaneously. For example, one such idea of an ultra-wide bandgap metasurface has been published recently [34] which uses destructive interference rather than local resonance to create ultra-wide bandgaps starting from lower frequencies and hence addresses the abovementioned contradictions (ii) and (iii). Another concept using smaller resonators [27] has also been presented recently which is effective in the range of 50–100 Hz, addressing contradiction (i). In this research, we propose and study a meta-surface concept that attempts to address simultaneously all of these contradictions, with the main focus on contradiction (i), (ii), and (iii) and partially on (iv). Such a metamaterial can be constructed above-ground and can produce wide bandgaps while consisting of resonators that are of feasible size at a human scale.

To present this new concept as a viable option, we have investigated the proposed metasurface numerically using finite element simulations and studied their bandgap and frequency-domain performance. This is the commonly and widely used simulation methodology for this kind of study [11, 21, 40, 50–54]. We have also carried out a time-transient study for the seismic waves, in the lowest end of the bandgap frequency range, to further validate and interpret the results of bandgap and frequency-domain analysis. The prime objective of this study is the creation of low-frequency, wide bandgaps for Rayleigh surface waves using relatively smaller and shorter resonators periodically placed above ground in metasurface configuration.

2. Metasurface design

The metasurface studied in this research has been conceived as a periodic array of capped pillars with pad footing placed on the ground. The capped pillars act as resonators and undergo local resonance by their resonant frequencies when interacting with seismic surface waves (Rayleigh waves in this case) and act as a barrier for a broad range of wave frequencies. Thus, each capped pillar resonator (CPR) is a component of the metasurface unit cell, and such unit cells are the

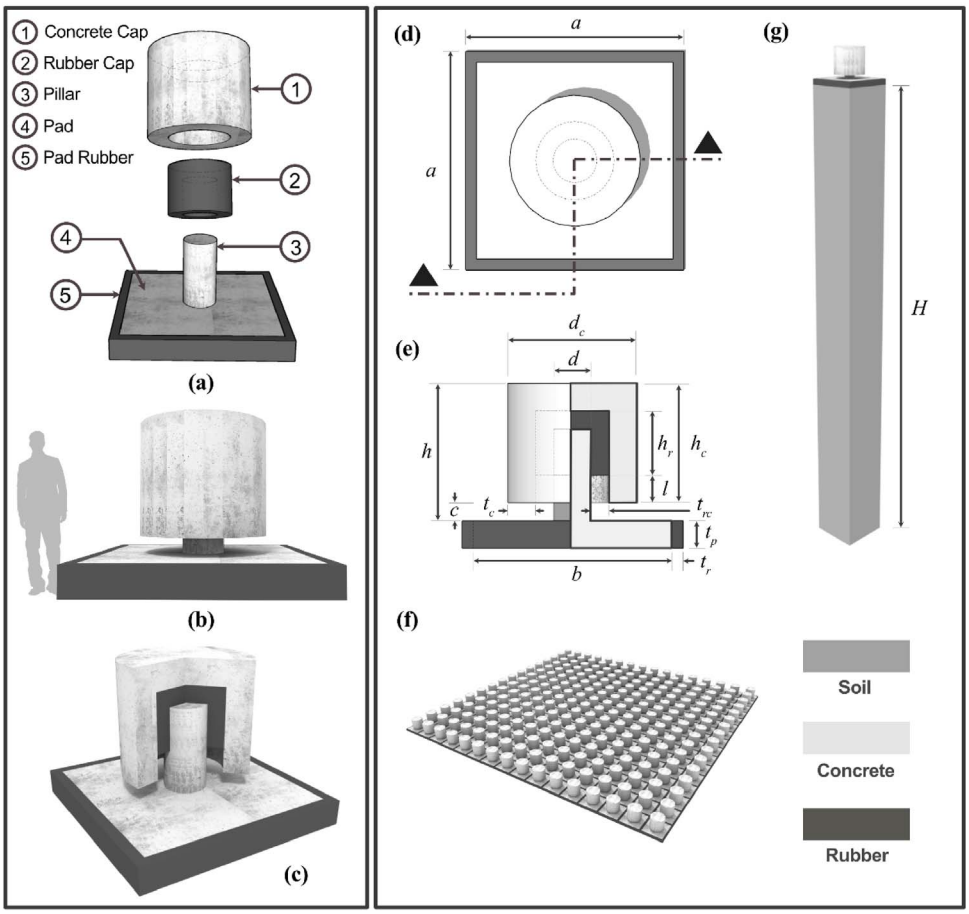

Figure 1. Assembly and schematic diagrams of CPR metasurface with necessary geometric details (a) exploded view of the CPR (b) assembled view of the CPR along with the average human dimensions to have an idea of size and scale (c) view of the CPR with a pie slice removed to expose the inner assembly (d) top view of CPR (e) sectional view of CPR which should be viewed in conjunction with Table 1 (f) CPR periodic arrangement for 15×15 resonators (g) complete unit cell for band structure analysis consisting of CPR and soil block.

fundamental building blocks of this metasurface. Moreover, the CPRs are assumed to be perfectly attached to the ground. For practical applications, such conditions can be achieved by anchoring to the ground.

The CPR consists of a round concrete (which implies reinforced concrete in this article) pillar supported on a rectangular concrete pad footing which in turn rests on the ground. The pillar bears over itself a construction grade rubber [55] cap and concrete cap respectively. Moreover, the gap between the two pads is filled with a layer of the same rubber. The details of this assembly are shown in Figure 1(a–c) along with the geometric details in Figure 1(d,e) and Table 1. Material properties are given in Table 2. A typical periodic arrangement of the resonators is shown in Figure 1(f). The unit cell of this metasurface consists of CPR and a cuboidal soil block of sufficient height to simulate surface waves.

Table 1. Geometric parameters

Parameter	Value (mm)	Description
a	2500	Lattice parameter
b	2250	Size of pad
c	200	Concrete cap clearance from pad
d	500	Diameter of pillar
d_c	1500	Outer diameter of concrete cap
H	24,700	Height of soil block
h	1500	Height of resonator above ground
h_c	1300	Height of concrete cap
h_r	700	Height of rubber cap
l	300	Unfilled height of concrete cap
t_c	300	Thickness of concrete cap
t_p	300	Thickness of pad
t_r	125	Thickness of pad rubber
t_{rc}	200	Thickness of cap rubber

Table 2. Material properties

Material property	Concrete	Rubber	Soil
Density, ρ, (kg/m^3)	2500	1300	1800
Young's modulus, E, GPa	30	0.001375	20
Poisson's ratio, ν	0.35	0.463	0.3

3. Modeling and simulation

To investigate the wave attenuation behavior of the proposed metasurface, a three-pronged methodology has been adopted using finite element analysis. Firstly, the band structure analysis is conducted for a single unit cell by applying the Floquet–Bloch theorem. Then, the transmission loss is investigated by performing a 2D frequency sweep analysis in the frequency domain for a model consisting of a finite number of unit cells arranged as an array and constrained using Perfectly Matched Layer (PML) [56, 57]. Finally, the time-transient analysis is carried out to study the wave propagation behavior of the system in the time domain. Of these three strategies, the first one predicts the wave propagation behavior of a spatially infinite periodic medium based on the behavior of a single unit cell which is an ideal case and not to be encountered in practice. Hence, for practical purposes, a periodic medium consisting of a finite number of unit cells is simulated in the latter two procedures. The modeling and simulation methodology has been detailed in Sections 3.1 and 3.2. For all the analyses, COMSOL Multiphysics software has been used. All the materials are assumed to be linear, elastic, homogeneous, and isotropic. However, geometric nonlinearities have been taken into account for band structure and frequency-domain analyses.

3.1. *Modeling for bandgap analysis*

The capped pillar metasurface (CPMS) studied in this article is a periodic structure that consists of spatially periodic unit cells as shown in Figure 1(g). These unit cells are analogous to the primitive unit cells of the crystal lattice (Bravais lattice) in solids. The primitive unit cells in Bravais lattice, or simply the unit cells, are the smallest representation of the lattice structure

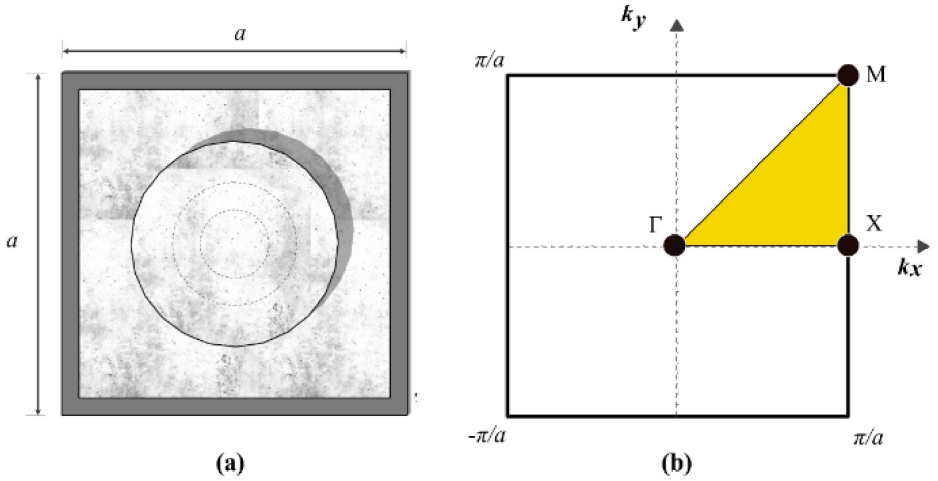

Figure 2. Brillouin Zone (a) top view of the unit cell for Bravais lattice (b) First Brillouin Zone (FBZ) showing the Irreducible Brillouin Zone (IBZ) as shaded.

(periodic structure) and are constructed by studying the translational symmetry of their spatial distribution. In a periodic structure, a square unit cell having the size $a \times a$ in the x–y plane will be spatially repeated after every a distance in both directions of the plane. This a is called the lattice constant or lattice parameter. In such periodic structures, the wave propagation can be studied by applying Floquet–Bloch boundary conditions, that exploit the spatial periodicity of the lattice, crystal, or periodic medium, and thus simplifying and reducing the problem to an eigenvalue problem. The general mathematical form of the Floquet–Bloch theorem is [58]

$$\psi_K(r) = \mathrm{e}^{\mathrm{i}K\cdot r}\, u_K(r), \tag{1}$$

where r is the position vector, $\psi_k(r)$ is the Bloch wave function or the Bloch wave, $u_k(r)$ is a periodic function having the same periodicity as the Bravais lattice and can vary depending on the value of K, which is indicated by its appearance in the index. K is the wavevector in reciprocal lattice having components k_x and k_y in x and y directions for a planar case. The periodic function $u_k(r)$ can be written as

$$u_k(r) = u_k(r + R). \tag{2}$$

Here, R is a lattice parameter that, in our case, equals a. Thanks to this theorem, now, we just need to investigate the eigenfrequency dynamics of a single unit cell in reciprocal space i.e., Brillouin Zone (usually the First Brillouin Zone or FBZ) and its results can be extrapolated to the whole periodic domain using the theorem. This problem, computationally, can be further simplified owing to the geometric symmetries of Brillouin Zone when we obtain Irreducible Brillouin Zone (IBZ), as shown in Figure 2(b). Now, just by sweeping Bloch wavevector K along the perimeter of IBZ, ΓXM, the eigenfrequencies can be determined.

To set up the model for bandgap analysis using the finite element method, the Floquet–Block Boundary conditions are applied on the four lateral faces (i.e., in x and y directions) of the pad rubber (t_p) and soil block (H) parts of the unit cell shown in Figure 1(e,g). The bottom face is applied with fixed boundary conditions. Then, by parametrically sweeping the wavevector along the perimeter of IBZ i.e., ΓXM, the eigenfrequencies are determined for each step value of wavevector from $(0, 0)$ to $(\pi/a, 0)$, $(\pi/a, 0)$ to $(\pi/a, \pi/a)$ and $(\pi/a, \pi/a)$ to $(0, 0)$. The data from this study is then used for dispersion analysis of the metamaterial which gives us the band structure

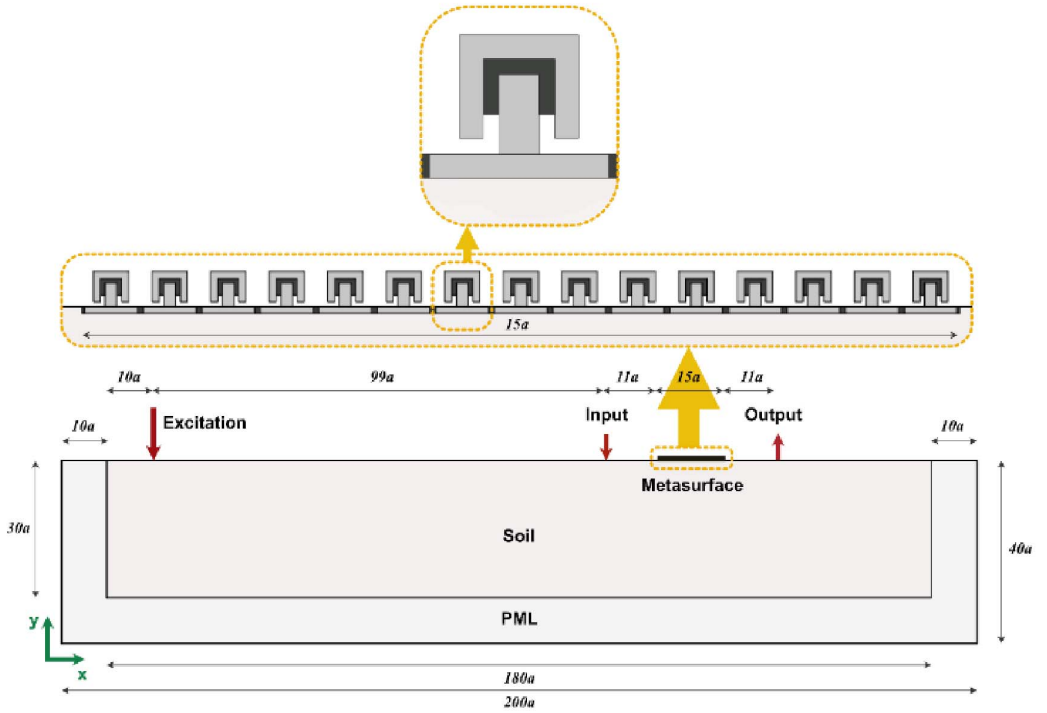

Figure 3. Simulation model with a finite number (15) of CPRs for transmission/frequency-domain analysis.

and bandgaps. The band structure is the plot of eigenfrequencies against the wavevector. To separate surface waves from body waves, the sound cone method [40, 51, 59, 60] is used.

3.2. *Modeling for attenuation analysis*

3.2.1. *Frequency-domain study*

While band structure analysis predicts the behavior of infinitely periodic structures, in the real-world, such systems have to be geometrically finite with a finite number of unit cells. Such finite arrangement has to attenuate the transmission of bandgap frequencies up to the desirable limits. Transmission and its loss for Rayleigh waves can be determined in the frequency domain by modeling the system as shown in Figure 3. The 2D model consists of a $180a \times 30a$ soil domain having a $10a$ wide PML layer on the left, right, and bottom sides. This PML makes sure that no waves are reflected from the boundaries. Furthermore, the whole model has been restrained by low-reflecting boundaries on the left, right, and bottom sides. To simulate the Raleigh wave response, excitation in the form of unit prescribed displacement has been applied at a distance $10a$ from the top left corner of the soil domain, as shown in Figure 3.

The metasurface is placed at $110a$ from the excitation point. A typical such arrangement for 15 CPRs can be seen in Figure 2. Dimensions of the CPR are the same as for its 3D counterpart in Section 3.1. For the transmission or transmittance analysis, a step-by-step frequency-domain study has been carried out for the applied excitation and by sweeping the frequency from 0.01 Hz to 20 Hz. The model has been meshed in such a manner that the maximum element size does not exceed $a/3$. The input response in the form of displacement amplitude has been recorded at $99a$ from the excitation point and the output response has been probed at a distance $11a$ from

the right-side edge of the metasurface. These responses are used to calculate transmission of the wave amplitude through the region where metasurface has been applied and can give the idea of metasurface performance in terms of transmission loss. The results of this analysis have been presented in Section 4.2.

For a comprehensive parametric picture, this analysis has been further expanded for 30 CPRs and for the 2× and 3× increase in concrete cap mass to investigate the effect of these variations on the transmission. Moreover, analysis has also been repeated to study the performance of metasurface for different shear wave speeds.

3.2.2. *Time-transient study*

For the time-transient study, the same geometry of 2D model as shown in Figure 3 has been used. In this case, waves have been generated using a Ricker wavelet [61] as the excitation force which is commonly used in seismology for simulation seismic wave loadings. The time function of this wavelet is

$$g(t) = A_0[2(\pi f_0(t-t_0))^2 - 1]\mathrm{e}^{-[\pi f_0(t-t_0)]^2}, \tag{3}$$

where A_0 is the amplitude and the parameter $t_0 = 1$, whereas, f_0 is the dominant frequency of the signal and has been chosen from the lower bound of the bandgap from bandgap analysis i.e., 8 Hz. The maximum size of the mesh elements has been selected as $a/4$ while time step size has been chosen as $1/(60 \times f_0)$, where f_0 is the central frequency of the wavelet. The results of this analysis are discussed in Section 4.3. This analysis also gives a picture of wave propagation modes and their interaction with the metasurface. The same has also been discussed in Section 4.3.

4. Results and discussions

4.1. *Band structure*

Analysis of the unit cell under Floquet–Bloch boundary condition as detailed in Section 3.1 determines the band structure of the metasurface which can be depicted graphically by plotting the eigenfrequencies of the unit cell against the Bloch wavevector. In this analysis, we have used a reduced wavevector (obtained by multiplying the wavevector K with the factor a/π) with an incremental step of 0.05 and analyzed for the first 20 eigenfrequencies. The plot between the reduced wavevector and eigenfrequencies shows all the eigenmodes of the metasurface unit cell for the respective eigenfrequencies. However, it is to be mentioned that the applied excitation load generates both the body waves and surface waves. And these waves excite different modes in the unit cell. To correctly gauge the performance of the unit cell, it is important to separate the surface modes from the body modes. In other words, it is required to filter the frequencies which only excite the resonant frequencies of CPR (the surface waves). For the extraction of these modes, the sound cone method has been used in which a curve is plotted for the lowest elastic wave velocity in the soil domain which is the shear wave velocity. The sound cone curve partitions the dispersion or band structure plot into a region that inhabits surface wave modes (region below the red-lined curve) and a region in which the body wave modes exist (shaded region above the curve as shown in Figure 4). If f is the frequency, v^s_{soil} is the velocity of shear wave in the soil, the sound cone curve is obtained as

$$f = (K \cdot v^s_{\mathrm{soil}})/2\pi \tag{4}$$

$$K = \sqrt{k_x + k_y} \tag{5}$$

$$v^s_{\mathrm{soil}} = \sqrt{G_{\mathrm{soil}}/\rho_{\mathrm{soil}}}, \tag{6}$$

where ρ_{soil} is the density and G_{soil} is the shear modulus of soil.

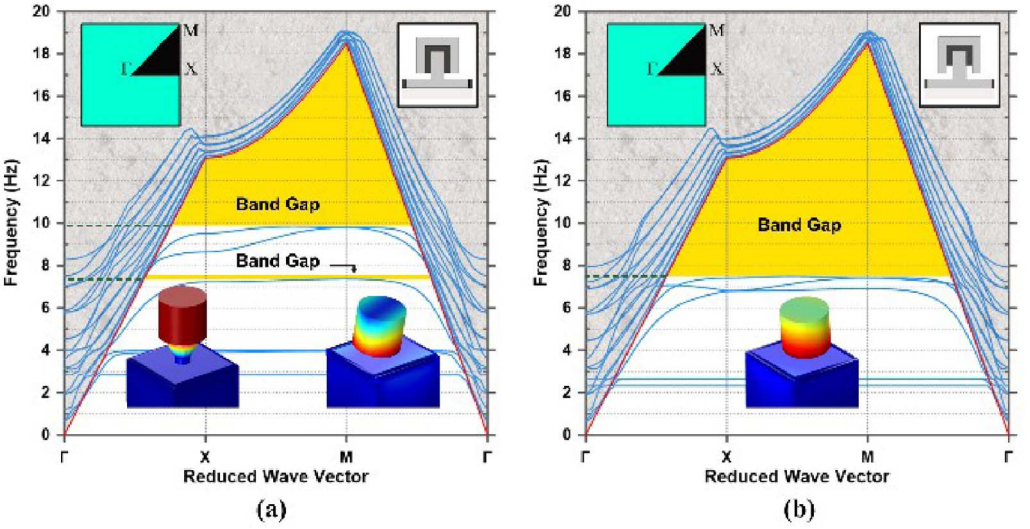

Figure 4. Band structure diagrams for (a) CPR with full rubber cap (b) CPR with reduced rubber cap.

Periodic placement of the CPRs causes wave dispersion which can be understood by studying the band structure of the metasurface, which was shown in Figure 4. Figure 4(b) shows the results of our bandgap analysis on the proposed unit cell in Figure 1. For comparison, an analysis of the unit cell having the rubber cap up to the rim of the cap has also been carried out. It can be seen that the CPR with a full rubber cap has two bandgaps. One is very thin at 7.37 Hz and a wider one starting from 9.80 up to 18.61 Hz. However, the CPR with reduced cap rubber height shows a single wide bandgap from 7.43 to 18.58 Hz. This is because of the reduction in stiffness of the system. The system essentially behaves like a mass-in-mass system [62, 63] but with additional degrees of freedom due to the configuration of cap mass around the pillar. This can be seen from the mode shape of the CPR in Figure 4b. The is the eigenmode shape of the CPR which is invoked at the eigenfrequency of 7.43 and causes the wide bandgap for frequencies up to 18.58. It is to be emphasized that the main bandgap mechanism for this system, in this case, is the energy trapping [64,65] and not the damping. Changes in the topology of cap rubber can further improve the bandgap performance which, however, is outside the scope of this article.

4.2. *Transmission*

To test the validity of the bandgap results for the finite CPMS (15 CPRs), a comprehensive transmission analysis comprising of a frequency sweep study is carried out in the frequency domain. The results in the form of the response of the system for the frequency range from 0.01 to 20 have been presented as transmission plots, as shown in Figures 5 and 6. The transmission can be calculated as

$$\text{Transmission (dB)} = 10\log_{10}\left(\frac{d_{\text{output}}}{d_{\text{input}}}\right), \tag{7}$$

where d_{output} is the displacement amplitude at output point (Figure 3) and d_{input} is the displacement amplitude at the input point shown in Figure 3. For a comprehensive parametric investigation of wave attenuation performance of the metasurface, the transmission analysis has been carried out for different number of CPRs, different concrete cap mass, and different seismic shear and longitudinal wave speeds.

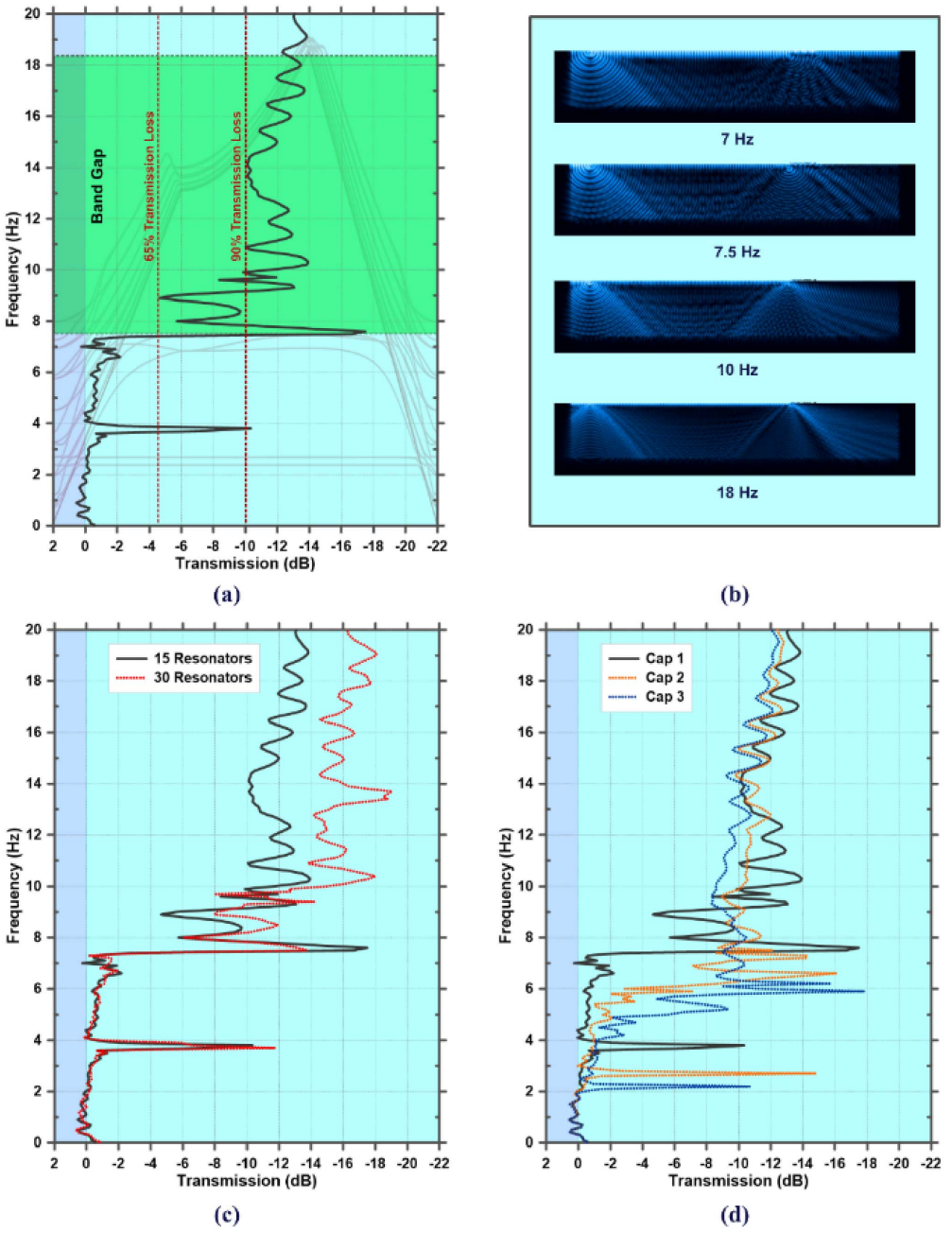

Figure 5. Transmittance plots for (a) 15 CPRs (b) total displacement at different frequencies (c) 30 CPRs (d) different concrete cap masses.

Figure 5 shows the wave amplitude transmission for all the CPMS material parameters mentioned in Table 2. We can call this CPMS the default CPMS. From these soil parameters, the shear wave and longitudinal wave frequency can be determined as approximately 65 and 122 m/s, respectively, and Rayleigh wave frequency as 60 m/s. Figure 5(a) is the transmission plot for

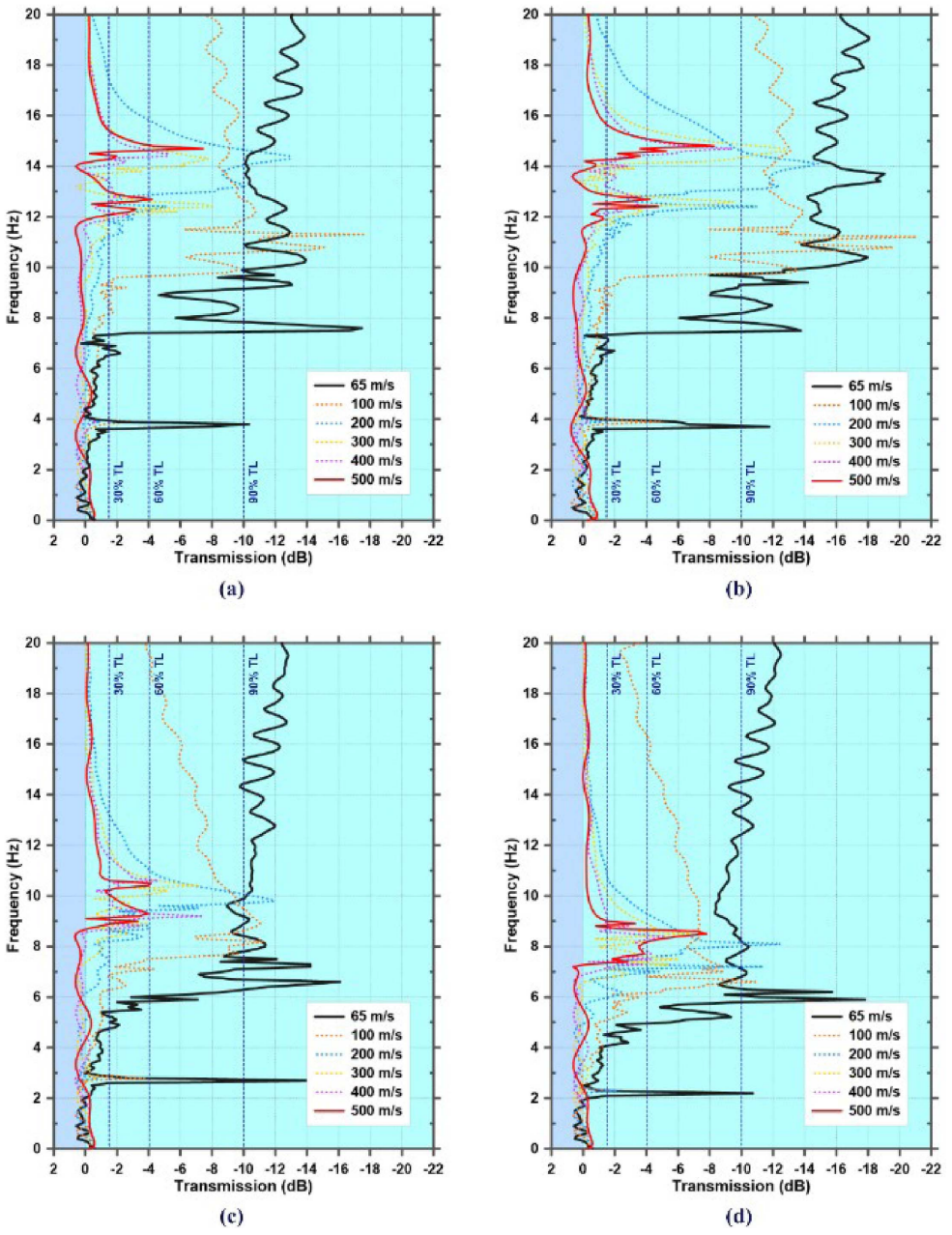

Figure 6. Transmittance plot at various shear wave speeds for (a) 15 CPRs (b) 30 CPRs (c) Cap I configuration (d) Cap 2 configuration.

the default CPMS having 15 CPRs only. The plot overlays the bandgap diagram from Figure 5(b). We can see that the wave transmission suddenly drops at 7.5 Hz as predicted in the band structure analysis. From 9 Hz onwards in the bandgap region, we can see that there is more than 90% transmission loss. Overall, there is at least a 65% transmission loss for this whole attenuation zone. The results can be further interpreted in the light of Figure 5(b) which shows the dispersion of waves

in terms of total displacement. At 7 Hz, just before the initiation of the attenuation zone, most of the wave energy transmits through the metasurface and amplitude decay is very small. A very small content of wave energy, however, transforms into body waves and can be seen propagating within the soil domain. At 7.5 Hz, just after the start of the bandgap, there is a sudden drop in the displacement amplitude beyond the right side of the metasurface. Here, almost all of the surface waves have transformed into body waves. However, we see some scattering of the body waves on the right side of the metasurface also which caused the reflection of some surface wave content back toward the source as surface waves. At 10 Hz, we observe that there is more body wave content propagation on the left side of the metasurface as compared to the 7.5 Hz waves. As the wave frequency changes, such backscattering also decreases, and at 18 Hz, it is minimal.

4.2.1. *Attenuation performance for increase in number of resonators*

To investigate the effect of an increase in the number of CPRs, transmission studies are carried out for 30 resonators. The transmission plot for this case has been shown in Figure 5(c). The plot shows that with the increase in the number of resonators, there is an overall increase in transmission loss (decrease in transmission). As the bandgap analysis is carried out for infinite medium, there should be further loss in transmission with a further increase in the number of resonators.

4.2.2. *Attenuation performance for concrete cap mass*

The natural frequencies of a system depend on the mass and stiffness. An increase in the resonating mass is expected to lower the resonant frequencies and bandgaps are supposed to start at lower frequencies.

To study this effect, the analysis was carried out for three different cap masses. Cap 1 has the default mass according to the default material and geometric parameters selected in Section 2. Cap 2 and Cap 3 have 2× and 3× the mass of Cap 1, respectively. To simulate this mass increase, the density of the cap material is varied. However, the same effect can be achieved by varying the geometry of the cap. Figure 5(d) shows the effect of this mass variation. The effect with the increase in resonating mass can be seen.

4.2.3. *Attenuation performance for different shear wave speeds*

The performance of the seismic metamaterial system also depends upon the shear wave speed in the soil which in turn depends on the mechanical properties of the soil and dictates the velocity of Rayleigh waves. The metasurface system has also been simulated for different shear wave speeds i.e., 100 m/s, 200 m/s, 300 m/s, 400 m/s, and 500 m/s. The corresponding longitudinal wave speeds are calculated as 1.88× shear wave speeds based upon the ratio of soil density and Poisson's ratio of 1.88 which is assumed to remain constant. The results are shown in Figure 6. For a CPMS with 15 CPRs, we see in Figure 6(a) that as the shear wave speed increases, the transmission loss decreases for the same system specifications.

Assuming the shear wave speed in the upper 20 to 30 m of soil as 100 to 300 m/s [27], we can see that the effectiveness of metasurface decreases considerably when shear wave speed is above 200 m/s. Moreover, the threshold of the lowest frequency bandgap also rises. In this case, for a 60% transmission loss, the bandgap width for 300 m/s is about 1.4 Hz, for 200 m/s it is 3 Hz and for 100 m/s, it is a very wide band. If we increase the number of resonators to 30, as in Figure 6(b), we see that the transmission loss increases for all wave speeds. The bandgap width for 60% transmission loss for 300 m/s is now about 1.8 Hz in the range of 14.1 to 15.5 Hz, and 12.4 to 12.8 Hz. For 200 m/s, the total bandgap width for 90% transmission loss is now about

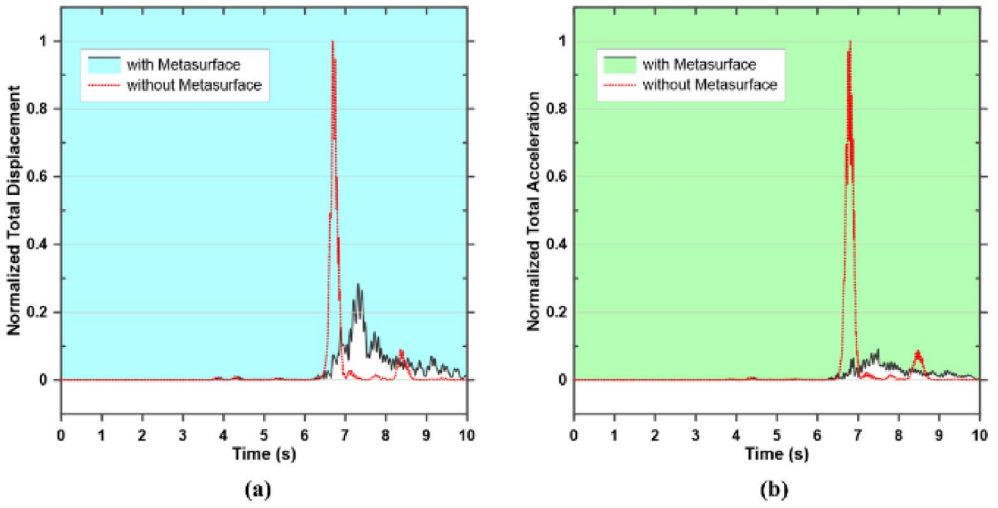

Figure 7. Time-domain plots at dominant excitation frequency of 8 Hz for (a) total normalized displacement (b) total normalized acceleration.

2 Hz while for 60% transmission loss, it has widened up to 4.5 Hz in the ranges 12.1–12.5 Hz and 12.9–16.9 Hz.

A study on the increase in the cap mass shows that the threshold resonant frequency lowers with the increase in this mass, resulting in an attenuation zone starting at a lower level. The results for Cap I and Cap 2 are shown in Figure 6(c) and (d), respectively. In this case, we see that while the threshold lower frequency is reduced, the transmission performance of lower speed shear waves i.e., 65 m/s and 100 m/s also get affected negatively.

4.3. *Time-transient behavior*

Based on the simulation model discussed in Section 3.2.2, a time-transient analysis has been carried out for the dominant excitation frequency of 8 Hz for the simulation time of 10 s. The results are presented in the form of normalized total displacement and normalized total acceleration against time in Figure 7. The 2D wave propagation screengrabs at various times have been shown in Figure 8.

We can see in Figure 7(a) that there is up to 70% decrease in the total displacement while Figure 7(b) shows up to 90% reduction in the total acceleration due to CPMS placement. If we see these plots in conjunction with Figure 8 (for qualitative comparison and clarity, see Figure A1 in the Appendix which has been plotted using smaller color range and hence shows more enhanced propagation pattern), we see that the Rayleigh wave created by wavelet reaches the metasurface after 5.5 s (at about 5.65 s). At 6 s, we see that the metasurface deflects some of the wave energy towards the soil as body waves while the remaining energy is trapped by each successive resonator and re-released, thus causing the decay in the amplitude. This behavior is more pronounced at 7 s. Now we can see that some of the waves have been reflected back towards the source while the metasurface resonators trap the energy and re-release it as body waves and Rayleigh waves which go through the same process at the next resonator. The capture and re-release mechanism are the main reasons for the attenuation at the lower end of the frequency spectrum. We see this re-release mechanism with reduced amplitude waves continuing till about

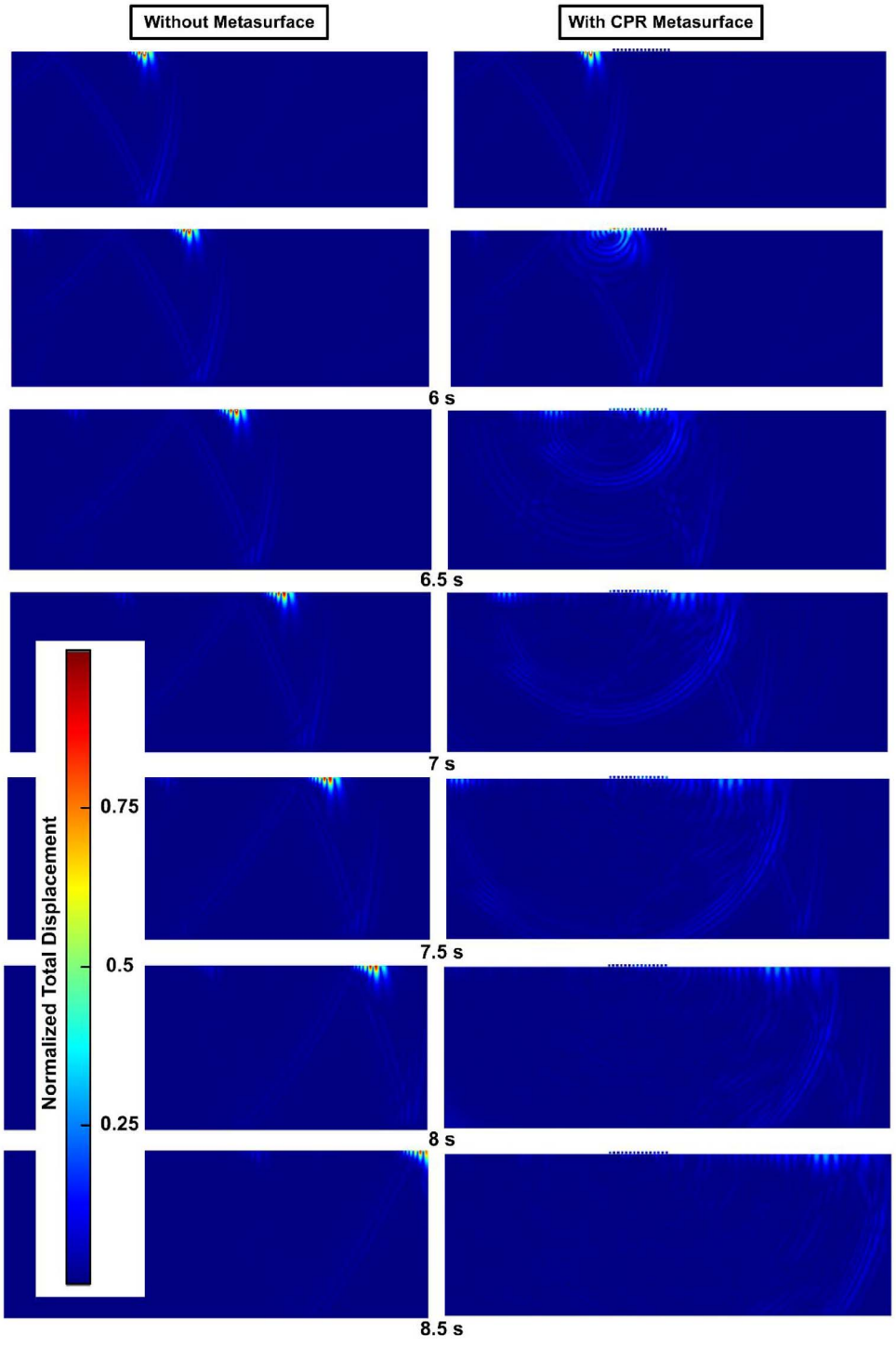

Figure 8. Instant total displacement at various wave propagation times (also see Figure A1 in Appendix).

8.5 s. It is also to be noted that the waves reflected towards the source are also of low amplitude. Moreover, Figure 8 shows that the value of total displacement has significantly reduced, in agreement with Figure 7(a), after transmission through the CPRMS.

5. Conclusions

Keeping in view the seismic metamaterial design contradiction introduced in Section 1, a metasurface with CPRs was proposed, designed, and analyzed numerically for bandgaps, transmission, and time-transient wave propagation at low frequency. The following conclusions have been drawn from the analysis:

(i) CPMS with the relatively smaller resonators (CPRs) produces wide bandgaps for the frequencies in the range of 7.5–18.5 Hz and thus can be used as seismic metasurface to protect the civil engineering structures against the low-frequency seismic vibrations.
(ii) A metasurface consisting of just 15 resonators can cause wave transmission loss of up to 90% for low-velocity Rayleigh waves in a wide-frequency band. Increasing the number of resonators can decrease transmission even further.
(iii) Increasing the mass of the resonator cap can lower the threshold frequency of bandgap initiation. Thus, it can be optimized according to the natural frequencies of the structures to be protected.
(iv) With the increase in the shear wave speed and in turn Rayleigh wave speed, the performance of the same metasurface is affected negatively. However, it still can offer sufficient attenuation for a limited number of resonators for the wave speeds in the top layer of soil.
(v) The analysis shows that for the effectiveness against higher velocity waves for wide bandgaps, lower attenuation frequencies, and greater wave energy transmission loss, the CPR metasurface can be designed by tuning the cap rubber geometry, the mass of the cap, and the number of resonators to achieve the desirable results.

This research addressed all the four design contradictions and showed that concepts similar to the one proposed in this article can be promising for the feasible design of seismic metasurfaces.

Availability of data and material

Not applicable.

Code availability

Not Applicable.

Conflicts of interest

The authors declare that they have no known competing financial interests or personal relationships that could have appeared to influence the work reported in this paper.

Funding

This research was supported by the National Natural Science Foundation of China (Grant No. 51978550).

Appendix

Figure A1. Qualitative wave propagation behavior at various propagation times (left) without metasurface, (right) with CPR metasurface.

References

[1] D. R. Smith, W. J. Padilla, D. C. Vier, S. C. Nemat-Nasser, S. Schultz, "Composite medium with simultaneously negative permeability and permittivity", *Phys. Rev. Lett.* **84** (2000), no. 18, p. 4184-4187.

[2] S. Krodel, N. Thome, C. Daraio, "Wide band-gap seismic metastructures", *Extreme Mech. Lett.* **4** (2015), p. 111-117 (in English).

[3] A. Labeyrie, "Hypertelescopes: the challenge of direct imaging at high resolution", in *New Concepts in Imaging: Optical and Statistical Models* (D. Mary, C. Theys, C. Aime, eds.), EAS Publications Series, vol. 59, EDP Sciences, Les Ulis, 2013, p. 5-23.

[4] M. B. Pu, P. Chen, Y. Wang, Z. Zhao, C. Huang, C. Wang, X. Ma, X. Luo, "Anisotropic meta-mirror for achromatic electromagnetic polarization manipulation", *Appl. Phys. Lett.* **102** (2013), no. 13, article no. 131906 (in English).

[5] M. Hamamda, G. Dutier, M. Boutismi, V. Bocvarski, J. Grucker, F. Perales, J. Baudon, M. Ducloy, "Atom "meta-optics": Negative-index media for matter waves in the nm wavelength range", in *2009 Conference on Lasers and Electro-Optics and Quantum Electronics and Laser Science Conference*, IEEE, New York, 2009, p. 2448-2449.

[6] Z. H. Jiang, C. Scarborough, D. H. Werner, P. L. Werner, C. Rivero-Baleine, C. Drake, "An isotropic 8.5 MHz magnetic meta-lens", in *2011 IEEE International Symposium on Antennas and Propagation (IEEE Antennas and Propagation Society International Symposium)*, IEEE, New York, 2011, p. 1151-1154.

[7] V. Galdi, V. Pierro, G. Castaldi, N. Engheta, "Genetically optimized metasurface pairs for wideband out-of-phase mutual response", *IEEE Anten. Wirel. Propag. Lett.* **7** (2008), p. 788-791 (in English).

[8] C. Boutin, L. Schwan, M. S. Dietz, "Elastodynamic metasurface: Depolarization of mechanical waves and time effects", *J. Appl. Phys.* **117** (2015), no. 6, article no. 064902 (in English).

[9] A. Colombi, D. Colquitt, P. Roux, S. Guenneau, R. V. Craster, "A seismic metamaterial: The resonant metawedge", *Sci. Rep.* **6** (2016), article no. 27717 (in English).

[10] S. H. Kim, M. P. Das, "Artificial seismic shadow zone by acoustic metamaterials", *Modern Phys. Lett. B* **27** (2013), no. 20, article no. 1350140 (in English).

[11] A. Palermo, S. Krodel, A. Marzani, C. Daraio, "Engineered metabarrier as shield from seismic surface waves", *Sci. Rep.* **6** (2016), article no. 39356 (in English).

[12] M. I. Hussein, M. J. Frazier, "Metadamping: An emergent phenomenon in dissipative metamaterials", *J. Sound Vib.* **332** (2013), no. 20, p. 4767-4774 (in English).

[13] F. Basone, M. Wenzel, O. S. Bursi, M. Fossetti, "Finite locally resonant Metafoundations for the seismic protection of fuel storage tanks", *Earthquake Eng. Struct. Dyn.* **48** (2019), no. 2, p. 232-252 (in English).

[14] B. Li, Y. Q. Liu, K. T. Tan, "A novel meta-lattice sandwich structure for dynamic load mitigation", *J. Sandwich Struct. Mater.* **21** (2019), no. 6, p. 1880-1905 (in English).

[15] R. M. Walser, "Electromagnetic metamaterials", in *Complex Mediums II: Beyond Linear Isotropic Dielectrics (Proceedings of the Society of Photo-Optical Instrumentation Engineers (SPIE))* (A. Lakhtakia, W. S. Weiglhofer, I. J. Hodgkinson, eds.), vol. 4467, SPIE-Int Soc Optical Engineering, Bellingham, 2001, p. 1-15.

[16] J. Li, C. T. Chan, "Double-negative acoustic metamaterial", *Phys. Rev. E* **70** (2004), no. 5, article no. 055602 (in English).

[17] X. M. Zhou, J. Hu, G. K. Hu, "Transparency effect induced by elastic metamaterials", in *Piers 2008 Hangzhou: Progress in Electromagnetics Research Symposium, Vols I and II, Proceedings (Progress in Electromagnetics Research Symposium)* (J. A. Kong, ed.), Electromagnetics Acad, Cambridge, 2008, p. 963-966.

[18] S. H. Kim, M. P. Das, "Seismic waveguide of Metamaterials", *Mod. Phys. Lett. B* **26** (2012), no. 17, article no. 1250105 (in English).

[19] S. Brule, E. H. Javelaud, S. Enoch, S. Guenneau, "Experiments on seismic metamaterials: Molding surface waves", *Phys. Rev. Lett.* **112** (2014), no. 13, article no. 133901 (in English).

[20] Y. Achaoui, T. Antonakakis, S. Brûlé, R. V. Craster, S. Enoch, S. Guenneau, "Clamped seismic metamaterials: ultra-low frequency stop bands", *New J. Phys.* **19** (2017), no. 6, article no. 063022.

[21] Y. Achaoui, B. Ungureanu, S. Enoch, S. Brule, S. Guenneau, "Seismic waves damping with arrays of inertial resonators", *Extreme Mech. Lett.* **8** (2016), p. 30-37 (in English).

[22] S. Krödel, N. Thomé, C. Daraio, "Wide band-gap seismic metastructures", *Extreme Mech. Lett.* **4** (2015), p. 111-117.

[23] C. P. Berraquero, A. Maurel, P. Petitjeans, V. Pagneux, "Experimental realization of a water-wave metamaterial shifter", *Phys. Rev. E* **88** (2013), no. 5, article no. 051002 (in English).

[24] T. C. Han, T. Yuan, B. W. Li, C. W. Qiu, "Homogeneous thermal cloak with constant conductivity and tunable heat localization", *Sci. Rep.* **3** (2013), article no. 1593 (in English).

[25] Y. Zeng, Y. Xu, H. Yang, M. Muzamil, R. Xu, K. Deng, P. Peng, Q. Du, "A Matryoshka-like seismic metamaterial with wide band-gap characteristics", *Int. J. Solids Struct.* **185** (2020), p. 334-341 (in English).

[26] Y. Zeng, P. Peng, Q.-J. Du, Y.-S. Wang, B. Assouar, "Subwavelength seismic metamaterial with an ultra-low frequency bandgap", *J. Appl. Phys.* **128** (2020), no. 1, article no. 014901.

[27] F. Zeighami, A. Palermo, A. Vratsikidis, Z. B. Cheng, D. Pitilakis, A. Marzani, "Medium-scale resonant wave barrier for seismic surface waves", *Mech. Based Des. Struct. Machines* **49** (2020), no. 8, p. 1157-1172 (in English).

[28] R. Zaccherini, A. Palermo, A. Marzani, A. Colombi, V. Dertimanis, E. Chatzi, "Mitigation of Rayleigh-like waves in granular media via multi-layer resonant metabarriers", *Appl. Phys. Lett.* **117** (2020), no. 25, article no. 254103 (in English).
[29] R. Zaccherini, A. Colombi, A. Palermo, V. K. Dertimanis, A. Marzani, H. R. Thomsen, B. Stojadinovic, E. N. Chatzi, "Locally resonant metasurfaces for shear waves in granular media", *Phys. Rev. Appl.* **13** (2020), no. 3, article no. 034055 (in English).
[30] X. Pu, A. Palermo, Z. Cheng, Z. Shi, A. Marzani, "Seismic metasurfaces on porous layered media: Surface resonators and fluid–solid interaction effects on the propagation of Rayleigh waves", *Int. J. Eng. Sci.* **154** (2020), article no. 103347.
[31] Muhammad, T. Wu, C. W. Lim, "Forest trees as naturally available seismic metamaterials: Low frequency Rayleigh wave with extremely wide bandgaps", *Int. J. Struct. Stability Dyn.* **20** (2020), no. 14, article no. 2043014.
[32] P. Mandal, S. N. Somala, "Periodic pile-soil system as a barrier for seismic surface waves", *SN Appl. Sci.* **2** (2020), no. 7, article no. 1184.
[33] M. Lott, P. Roux, S. Garambois, P. Gueguen, A. Colombi, "Evidence of metamaterial physics at the geophysics scale: the METAFORET experiment", *Geophys. J. Int.* **220** (2020), no. 2, p. 1330-1339 (in English).
[34] W. Liu, G. H. Yoon, B. Yi, Y. Yang, Y. Chen, "Ultra-wide band gap metasurfaces for controlling seismic surface waves", *Extreme Mech. Lett.* **41** (2020), article no. 101018.
[35] T. Li, Q. Su, S. Kaewunruen, "Seismic metamaterial barriers for ground vibration mitigation in railways considering the train-track-soil dynamic interactions", *Construct. Build. Mater.* **260** (2020), article no. 119936.
[36] A. Colombi, R. Zaccherini, G. Aguzzi, A. Palermo, E. Chatzi, "Mitigation of seismic waves: Metabarriers and metafoundations bench tested", *J. Sound Vib.* **485** (2020), article no. 115537.
[37] Y. Zeng, Y. Xu, K. Deng, P. Peng, H. Yang, M. Muzamil, Q. Du, "A broadband seismic metamaterial plate with simple structure and easy realization", *J. Appl. Phys.* **125** (2019), no. 22, article no. 224901 (in English).
[38] Y. Xu, R. Xu, P. Peng, H. W. Yang, Y. Zeng, Q. J. Du, "Broadband H-shaped seismic metamaterial with a rubber coating", *EPL* **127** (2019), no. 1, article no. 17002 (in English).
[39] F. F. Sun, L. Xiao, "Bandgap characteristics and seismic applications of inerter-in-lattice metamaterials", *J. Eng. Mech.* **145** (2019), no. 9, article no. 04019067 (in English).
[40] Muhammad, C. W. Lim, J. N. Reddy, "Built-up structural steel sections as seismic metamaterials for surface wave attenuation with low frequency wide bandgap in layered soil medium", *Eng. Struct.* **188** (2019), p. 440-451 (in English).
[41] Y. F. Liu, J. K. Huang, Y. G. Li, Z. F. Shi, "Trees as large-scale natural metamaterials for low-frequency vibration reduction", *Construct. Build. Mater.* **199** (2019), p. 737-745 (in English).
[42] A. Palermo, M. Vitali, A. Marzani, "Metabarriers with multi-mass locally resonating units for broad band Rayleigh waves attenuation", *Soil Dyn. Earthq. Eng.* **113** (2018), p. 265-277 (in English).
[43] A. Palermo, S. Krodel, K. H. Matlack, R. Zaccherini, V. K. Dertimanis, E. N. Chatzi, A. Marzani, C. Daraio, "Hybridization of guided surface acoustic modes in unconsolidated granular media by a resonant metasurface", *Phys. Rev. Appl.* **9** (2018), no. 5, article no. 054026 (in English).
[44] A. Palermo, M. Vitali, A. Marzani, IEEE, "A multi-mass metabarrier to protect buildings from seismic rayleigh waves", in *2017 11th International Congress on Engineered Materials Platforms for Novel Wave Phenomena*, IEEE, New York, 2017, p. 250-252.
[45] L. Brillouin, *Wave Propagation in Periodic Structures*, 2nd ed., Dover Publications, Inc., New York, 1953.
[46] Z. Y. Liu, X. Zhang, Y. Mao, Y. Y. Zhu, C. T. Chan, P. Sheng, "Locally resonant sonic materials", *Science* **289** (2000), no. 5485, p. 1734-1736 (in English).
[47] C. Kittel, *Introduction to Solid State Physics*, 8th ed., Wiley, Hoboken, NJ, 2004.
[48] M. Miniaci, A. Krushynska, F. Bosia, N. M. Pugno, "Large scale mechanical metamaterials as seismic shields", *New J. Phys.* **18** (2016), article no. 083041 (in English).
[49] G. Altshuller, *And Suddenly the Inventor Appeared: TRIZ, the Theory of Inventive Problem Solving*, 2nd ed., Technical Innovation Center, Inc., Worcester, MA, 1996.
[50] Q. J. Du, Y. Zeng, Y. Xu, H. W. Yang, Z. X. Zeng, "H-fractal seismic metamaterial with broadband low-frequency bandgaps", *J. Phys. D-Appl. Phys.* **51** (2018), no. 10, article no. 105104.
[51] M. Miniaci, A. Krushynska, F. Bosia, N. M. Pugno, "Large scale mechanical metamaterials as seismic shields", *New J. Phys.* **18** (2016), no. 8, article no. 083041.
[52] Muhammad, C. W. Lim, "Elastic waves propagation in thin plate metamaterials and evidence of low frequency pseudo and local resonance bandgaps", *Phys. Lett. A* **383** (2019), no. 23, p. 2789-2796.
[53] Y. Xu, R. Xu, P. Peng, H. Yang, Y. Zeng, Q. Du, "Broadband H-shaped seismic metamaterial with a rubber coating", *EPL (Europhys. Lett.)* **127** (2019), no. 1, article no. 17002.
[54] Y. Zeng, Y. Xu, H. Yang, M. Muzamil, R. Xu, K. Deng, P. Peng, Q. Du, "A Matryoshka-like seismic metamaterial with wide band-gap characteristics", *Int. J. Solids Struct.* **185–186** (2019), p. 334-341.

[55] V. La Salandra, M. Wenzel, O. S. Bursi, G. Carta, A. B. Movchan, "Conception of a 3D metamaterial-based foundation for static and seismic protection of fuel storage tanks", *Front. Mater.* **4** (2017), article no. 30 (in English).
[56] J.-P. Berenger, "A perfectly matched layer for the absorption of electromagnetic waves", *J. Comput. Phys.* **114** (1994), no. 2, p. 185-200.
[57] M. B. Duhring, V. Laude, A. Khelif, "Energy storage and dispersion of surface acoustic waves trapped in a periodic array of mechanical resonators", *J. Appl. Phys.* **105** (2009), no. 9, article no. 093504 (in English).
[58] P. Hofmann, *Solid State Physics: An Introduction*, 2nd ed., Wiley-VCH, Weinheim, Germany, 2015.
[59] Y. Achaoui, A. Khelif, S. Benchabane, L. Robert, V. Laude, "Experimental observation of locally-resonant and Bragg band gaps for surface guided waves in a phononic crystal of pillars", *Phys. Rev. B* **83** (2011), no. 10, article no. 104201 (in English).
[60] J. Huang, Y. Liu, Y. Li, "Trees as large-scale natural phononic crystals: Simulation and experimental verification", *Int. Soil Water Conserv. Res.* **7** (2019), no. 2, p. 196-202.
[61] D. Appelö, N. Petersson, "A stable finite difference method for the elastic wave equation on complex geometries with free surfaces", *Commun. Comput. Phys.* **5** (2009), p. 84-107.
[62] K. T. Tan, H. H. Huang, C. T. Sun, "Blast-wave impact mitigation using negative effective mass density concept of elastic metamaterials", *Int. J. Impact Eng.* **64** (2014), p. 20-29 (in English).
[63] X. C. Xu, M. V. Barnhart, X. P. Li, Y. Y. Chen, G. L. Huang, "Tailoring vibration suppression bands with hierarchical metamaterials containing local resonators", *J. Sound Vib.* **442** (2019), p. 237-248 (in English).
[64] H. H. Huang, C. T. Sun, G. L. Huang, "On the negative effective mass density in acoustic metamaterials", *Int. J. Eng. Sci.* **47** (2009), no. 4, p. 610-617 (in English).
[65] H. H. Huang, C. T. Sun, "Wave attenuation mechanism in an acoustic metamaterial with negative effective mass density", *New J. Phys.* **11** (2009), article no. 013003 (in English).